CHAPTER 4

SHIFT INVARIANT IMPROVED ADAPTIVE WAVELET FILTER (SIIAWF)

The homogeneity based variance estimation discussed in the previous chapter gives the local neighborhood information by calculating the differences in variances of two sub-regions. To obtain a more accurate local statistics, this chapter proposes two new local spatial adaptivity measures using the correlation of the wavelet coefficients. The method of determination of preliminary coefficient classification is modified using multiscale product for better identification of signal and noise coefficients. A new thresholding function is developed to reduce the fixed bias of soft thresholding and to reduce the number of coefficients in the zero zone.

This chapter describes the development of a new Shift Invariant Improved Adaptive Wavelet Filter (SIIAWF) with two new variance estimation techniques for the determination of adaptive threshold. The proposed SIIAWF is analyzed under two frameworks:

- SIIAWF^1 with an intra scale measure based variance estimation approach and
- SIIAWF^2 with a combined inter and intra scale dependency based variance estimation.

4.1 SHIFT INVARIANT IMPROVED ADAPTIVE FILTER[1] (SIIAWF[1])

Figure 4.1 illustrates the block diagram of the proposed shift invariant improved adaptive wavelet filter. A detailed explanation is given in following sections.

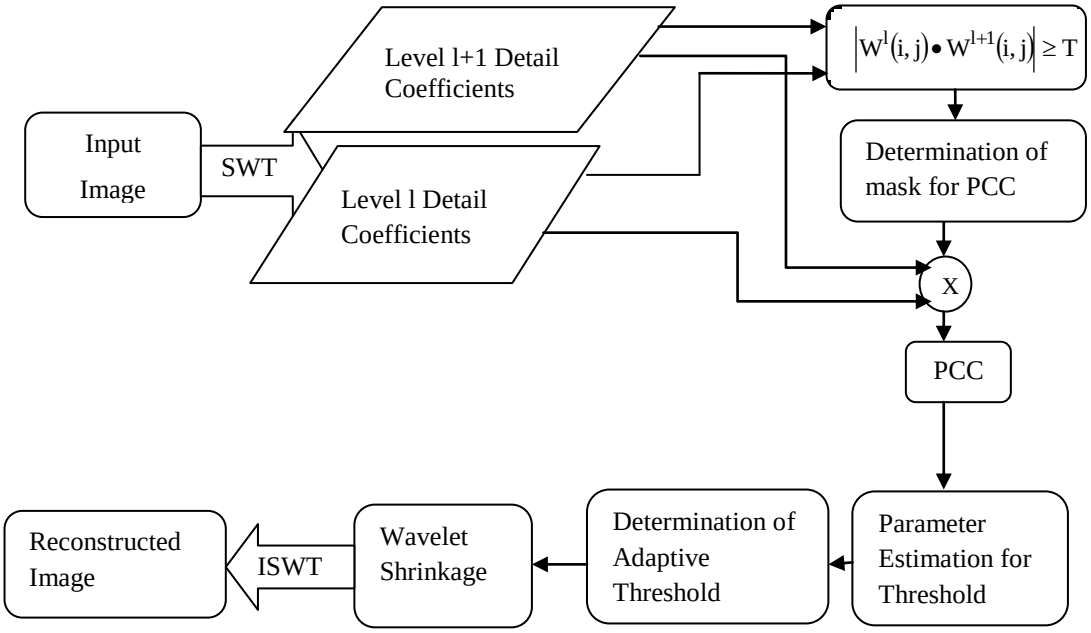

Figure 4.1 Block diagram of SIIAWF[1]

4.1.1 Preliminary Coefficient Classification (PCC)

The first step in the proposed algorithm is to determine a mask for each detail subband to identify the significant pixels of the image. The adjacent subband coefficient dependencies are utilized for this purpose. In wavelet decomposition, the dependencies among the wavelet coefficients are seen not only within the scales but also across the scales. In general, for the subbands with the same orientation the coefficients at particular spatial locations and adjacent scales exhibit a high correlation. It can be observed that the small magnitude parent coefficients at coarser scales are expected to yield insignificant children at finer scales. On the other hand, in the finer scale, the true signal coefficients which are said to have large magnitudes

probably have significant parents at coarser scales. However, the coefficients caused by noise would decay rapidly along scales (Liu & Moulin, 2001). This intra-scale and inter-scale dependency of the wavelet coefficients have been exploited by many authors for noise removal in digital images in different ways, as analyzed by Huysmans et al (2006), Duskunovic et al (2000), Bao & Zhang (2003). Xu et al (1994) determined the product of adjacent resolution scales of wavelet decomposition to enhance the edges and to weaken the noise content. Sadler & Swami (1998) analysed the product of multiscale wavelet coefficients and used them for the detection and estimation of step edges. Pizurica et al (2006) used a method for classification of signal of interest coefficients using inter scale product.

In the present approach, the product of the multi scale coefficients is used in a simpler way to estimate a mask for performing PCC. The mask denoted as $\hat{I}(i,j)$ contains a value either 0 or 1, depending on the degree of significance of each pixel which is determined using a rule given in Equation (4.1)

$$\hat{I}(i,j)=\begin{cases}0 & \left|W^{l}(i,j)\right|\left|W^{l+1}(i,j)\right| < \sigma_x^2 \\ 1 & \left|W^{l}(i,j)\right|\left|W^{l+1}(i,j)\right| \geq \sigma_x^2\end{cases} \tag{4.1}$$

where $W^{l}(i,j)$ is the wavelet coefficient at scale l and $W^{l+1}(i,j)$ is the wavelet coefficient at scale l+1. σ_x^2 is the signal variance estimated using Equation (4.2) for the subband under consideration.

$$\sigma_x^2=\frac{1}{MN}\sum_{i=1}^{M}\sum_{j=1}^{N}W^{2}(i,j) \tag{4.2}$$

The resultant mask $\hat{I}(i,j)$ gives a measure for the locations of signal of interest and noise coefficients for each detail image. Each detail subband is then

multiplied with its corresponding mask and the resultant subband matrix is used in the estimation of signal variance.

4.1.2 Intra-Scale Measure Based Signal Variance Estimation

The estimation of signal variance is a critical issue in any denoising scheme. It is estimated generally within a local window around the neighbourhood of each pixel using Maximum Likelihood (ML) or Maximum A Posteriori (MAP) estimate. As seen from the literature the incorporation of local spatial information of the subband coefficients, in signal variance estimation improves the performance of the denoising filters. The abrupt variation in gray level that denotes boundaries and edges bear essential information for improving human and machine interpretation. Hence incorporation of these details in variance estimation gives a better spatial adapativity. In the proposed approach, the abrupt changes in gray levels for each pixel location are determined by using an edge threshold. Jiang (2012) investigated that the lower and upper bounds of threshold for any data set are their mean and median respectively. The difference between the mean and the median of a finite data set is certainly not bigger than the mean absolute deviation of the data from the mean. A dynamic threshold which takes the value between these limits helps to locate the spatial characteristics of each pixel better. Utilizing this, the edge threshold is given in Equation (4.3)

$$\phi = \frac{1}{MN}\sum_{i=1}^{M}\sum_{j=1}^{N}\left(\left|W(i,j)-\mu\right|\right) \tag{4.3}$$

where μ is the mean of the sub-band under consideration and N is the number of pixels in the subband. The wavelet coefficients at different resolution scales are compared against this threshold and a LSAM is estimated as given in Equation (4.4)

$$E_T(i,j)=\begin{cases}0 & W(i,j)<\varphi \\ 1 & W(i,j)\geq\varphi\end{cases} \tag{4.4}$$

where $E_T(i,j)$ is the weight kernel defining the context and φ is the edge threshold. The estimated kernel serves as the LSAM for the pixels in the subband. Thus, the mean absolute deviation of the pixels from their subband mean gives an indication of the presence of an edge pixel (large magnitude pixel). The signal variance is then estimated as in Equation (3.6) by using σ_y^2 determined through Equation (4.5).

$$\sigma_y^2 = \frac{1}{MN}\sum_{i=1}^{M}\sum_{j=1}^{N} W^2(i,j)\bullet E_T(i,j) \tag{4.5}$$

where MN is the size of the image and $W(i,j)$ is the sub-band coefficient and $E_T(i,j)$ is the weight kernel. This proposed context based variance estimation lends a better adaptation to the filter performance than generally used ML method of estimation. This can be verified from the following Figures 4.2 and 4.3.

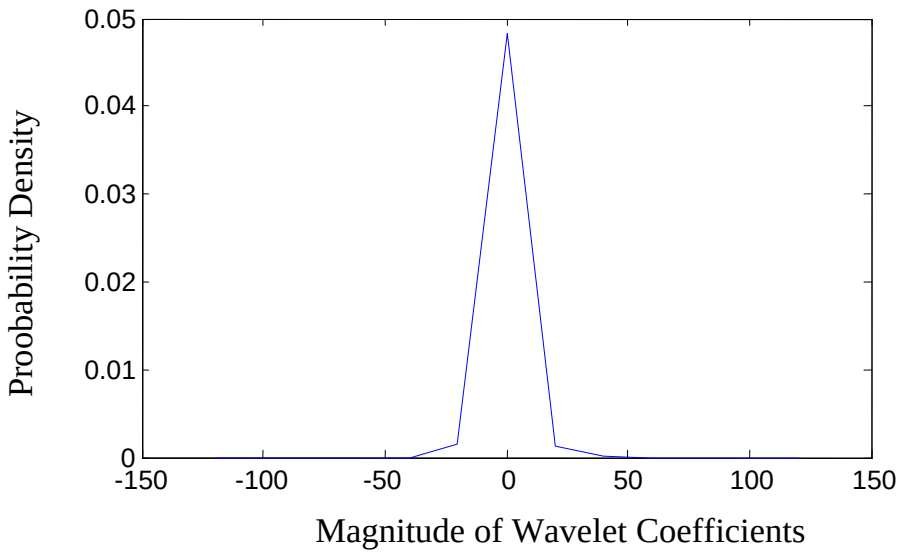

Figure 4.2 Histogram pdf of HH[1] subband

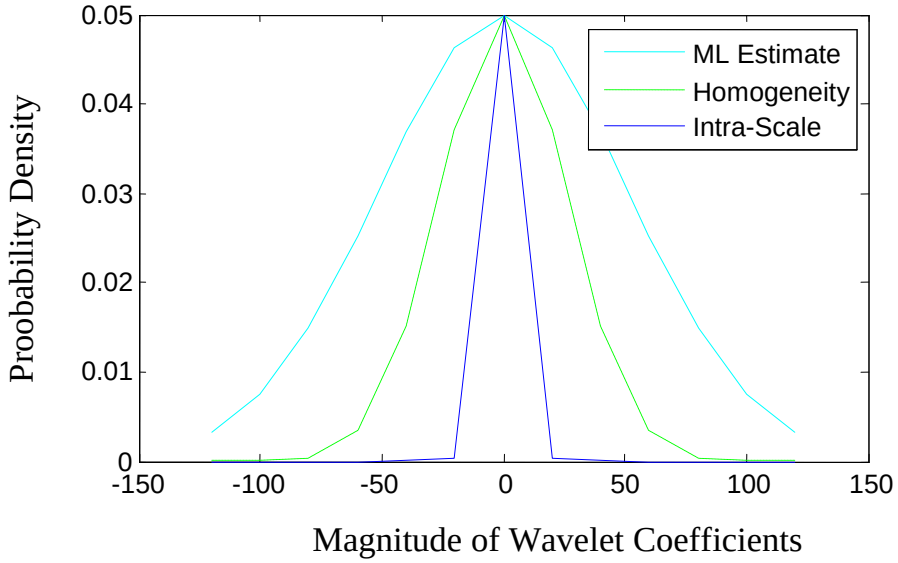

Figure 4.3 Comparison of pdfs' generated with ML estimate, homogeneity measure and intra-scale measure based variances

Figure 4.2 shows the pdf of the histogram of HH^1 subband and Figure 4.3 shows the pdf generated with calculated ML estimated variance, homogeneity measure based variance and the proposed intra-scale measure based variance. From the variance pdf's of Figure 4.3, it is obvious that the intra-scale based pdf fits better than the other two (ML and Homogeneity) variance pdf's. The signal variance thus estimated shows a good indication of the local variability of the coefficients.

The procedure is repeated for all the subband coefficients to calculate their signal variance and hence the threshold for all the subbands. After the estimation of signal variance, the adaptive threshold is determined as in Section 3.2.3.

4.1.3 New and Improved Adaptive Thresholding Function

The new and improved adaptive thresholding function proposed in Equation (4.6) aims at two improvements over soft thresholding and Qin et al (2010) approach. One possible improvement is in the direction of reducing further the fixed bias of the reconstructed coefficients with original coefficients and the second by reducing the number of zero coefficients. The proposed new and improved adaptive threshold function is defined as,

$$\begin{aligned}\hat{W}(i,j) &= \operatorname{sgn}(W(i,j))\left(|W(i,j)| - \left(\lambda_{MB} - \exp\left(\frac{-p}{|W_{max}(i,j)|^2 - \lambda_{MB}^2}\right)\lambda_{MB}\right)\right) && |W(i.j)| \geq \lambda_{MB} \\ &= W(i,j) - \mu(i,j) && \frac{\lambda_{MB}}{3} \leq |W_{i,j}| < \lambda_{MB} \\ &= 0 && \text{otherwise}\end{aligned} \tag{4.6}$$

where p is a positive constant. In the above equation $\hat{W}(i,j)$ is the denoised wavelet coefficient, $W(i,j)$ is the noisy wavelet coefficient, λ_{MB} is the adaptive threshold, $W_{max}(i,j)$ is the maximum wavelet coefficient of the subband under consideration. $\mu(i,j)$ is the mean estimator determined for individual coefficients in each subband by considering a local neighbourhood. The exponential weighting function, in Equation (4.6) helps in reducing the fixed bias. For $|W(i,j)| \geq \lambda_{MB}$, the adaptive thresholding function approximates soft thresholding function, when $p \to \infty$ and approximates hard thresholding when $p \to 0$. The proper selection of value of p improves the denoising performance. The parameter $W_{max}(i,j)$ in the denominator of the exponential weighting function helps in further reducing the fixed bias of the reconstructed coefficient. Figure (4.4) shows the performance of the proposed thresholding function compared with soft thresholding and Qin et al (2010) approach.

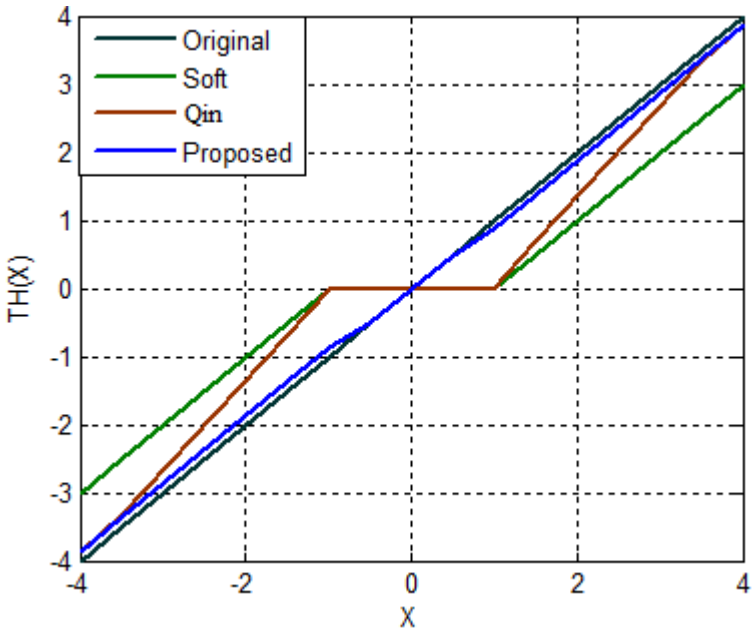

Figure 4.4 Comparison of thresholding function of SIIAWF[1] with soft thresholding and Qin et al approaches

From Figure 4.4, it is seen that the proposed thresholding function reduces the fixed bias of the soft thresholding function better than that of Qin et al (2010). Also it reduced the zero coefficients around the threshold. The reduction in fixed bias and the zero coefficients aid in keeping the important features of the original image, thus providing an improved noise reduction performance.

4.1.4 Summary of the Denoising Algorithm for SIIAWF[1]

The proposed wavelet denoising algorithm is summarized as follows:

Step 1: Compute the stationary wavelet transform for the input image to the required L resolution levels

Step 2: For each scale of decomposition 2^l, l= 1,2,…L-1 and for each orientation (HL, LH, HH)

- Determine the mask, $\hat{I}(i, j)$ using inter-scale dependency starting from the coarsest subband to finest subband using Equation (4.1)
- Multiply each detail subband with its corresponding mask
- Compute noise variance using Equation (3.2)
- Compute the signal variance using Equation (3.6) by
  * Computing the edge threshold using Equation (4.3)
  * Calculating the weight kernel using Equation (4.4)
  * Computing σ_y^2 as in Equation (4.5)
- Calculate the threshold T_{MB} using Equations (3.13) to (3.15)

Step 3: Apply thresholding using the shift invariant improved adaptive thresholding function as in Equation (4.6)

Step 4: Take inverse stationary wavelet transform.

4.1.5 Results and Discussion

The experimental set up, simulation environment and the input images are the same as detailed in section 3.3. The performance of SIIAWF[1] is compared with standard speckle filters like those of Frost, Kuan and Lee Filter, Soft thresholding, Qin et al (2010) and with EAWF discussed in chapter 3. Quantitative performance is measured with parameters like PSNR, MSE, SSIM, ENL and EPI. Visual quality enhancement is also compared. Simulations were carried out for synthetic phantom image and for clinical US images.

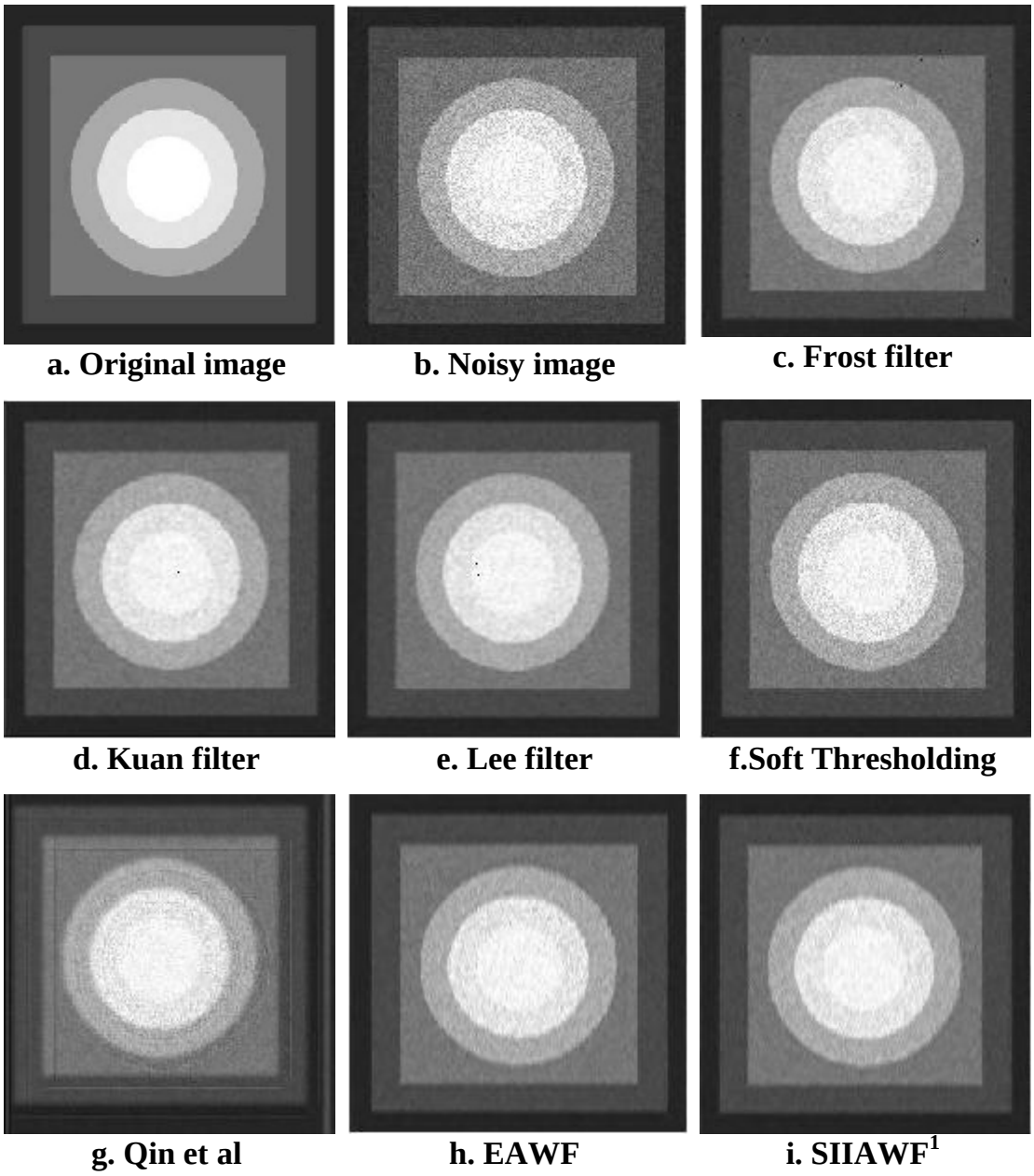

a. Original image **b. Noisy image** **c. Frost filter**

d. Kuan filter **e. Lee filter** **f.Soft Thresholding**

g. Qin et al **h. EAWF** **i. SIIAWF[1]**

Figure 4.5 Comparison of visual quality of SIIAWF[1] with existing filters for synthetic phantom image

Figure 4.5 shows the comparison of visual quality for a synthetic phantom image. Noisy phantom image is generated by introducing speckle artificially with 0.1 noise variance. The performance of this filter for noisy phantom input is as follows. The visual quality is seen to be improved compared to the standard speckle filters. Qin's approach in Figure 4.5(g)

shows a smoothed output with blurred edges. Noise removal of SIIAWF[1] is better than that of EAWF along with contrast enhancement.

Table 4.1 shows the quantitative performance comparison of various metrics of SIIAWF[1] with standard speckle filters, soft thresholding approach and EAWF.

Table 4.1 Performance comparison of SIIAWF[1] for different noise variances and filters

σ^2	Noisy	Frost	Kuan	Lee	Soft thresholding	Qin	EAWF	SIIAWF[1]
	Peak Signal To Noise Ratio							
0.01	34.9435	38.6438	39.8387	39.7923	36.2507	40.4068	41.8515	**42.2175**
0.04	31.4191	34.0636	35.5479	35.5193	33.1247	36.0805	38.4214	**38.5345**
0.08	30.4078	31.8946	32.9930	32.8841	32.0909	34.4780	36.4853	**36.8641**
0.1	30.1131	31.2677	32.0888	32.0758	31.7935	34.0053	35.7670	**36.4357**
	Mean Square Error							
0.01	20.8321	8.8859	6.7485	6.8211	15.4175	5.9210	4.2455	**3.9024**
0.04	46.8998	25.5104	18.1254	18.2455	31.6673	16.0335	9.3528	**9.1124**
0.08	59.1965	42.0362	32.6425	33.4712	40.1782	23.1889	14.6068	**13.3866**
0.1	63.3536	48.5639	40.1979	40.3180	43.0259	25.8553	17.2337	**14.7745**
	Structural Similarity Index Measure							
0.01	0.9663	0.9804	0.9819	0.9820	0.9666	0.9822	0.9848	**0.9854**
0.04	0.8882	0.9451	0.9512	0.9515	0.9135	0.9461	0.9608	**0.9612**
0.08	0.8104	0.9023	0.9145	0.9124	0.8559	0.9068	0.9346	**0.9377**
0.1	0.7815	0.8798	0.8944	0.8938	0.8311	0.8913	0.9210	**0.9285**
	Equivalent Number of Looks							
0.01	1.6661	1.7021	1.6975	1.6994	1.6419	1.7094	1.7114	**1.7131**
0.04	1.5483	1.6716	1.6844	1.6848	1.5643	1.6865	1.7125	**1.7204**
0.08	1.4127	1.6304	1.6648	1.6636	1.4767	1.6631	1.7081	**1.7286**
0.1	1.3606	1.6065	1.6564	1.6593	1.4347	1.6495	1.7013	**1.7247**
	Edge Preservation Index							
0.01	0.3274	0.2622	0.2244	0.2213	0.3486	0.5470	0.5766	**0.5979**
0.04	0.1722	0.1552	0.1646	0.1628	0.1759	0.2837	0.4285	**0.4417**
0.08	0.1239	0.1085	0.1312	0.1262	0.1221	0.1966	0.3598	**0.3659**
0.1	0.1114	0.0974	0.1100	0.1121	0.1072	0.1763	0.3308	**0.3387**

Table 4.2 Comparison of performance metrics of SIIAWF[1] for different wavelets

Wavelets / Metrics	dB4	Coif3	Sym2	haar	Bior 1.1
PSNR(dB4)	42.2175	41.8756	**42.7856**	40.1650	40.0661
MSE	**3.9024**	4.9878	4.5689	6.2601	6.4043
SSIM	**0.9854**	0.9852	0.9850	0.9825	0.9830
ENL	1.7131	1.7165	1.7152	1.7218	1.7241
EPI	**0.5979**	0.5678	0.5489	0.4076	0.4134

The performance of SIIAWF[1] is initially tested with different wavelet functions like daubechies, symlet, biorthogonal, haar and coiflet wavelet functions. The results are arranged in Table 4.2. From the results, it is seen that for sym2 wavelet function the PSNR value is high. But db4 gives higher SSIM and EPI values with comparable PSNR. Hence db4 is used for generating the results as seen in Table 4.1.

In Table 4.1 columns (3-5) show the performance measures of standard speckle filters. These filters are good at noise removal but lack in preservation of edge features. Column 6 gives the performance of soft thresholding approach. It shows an improvement in EPI measure indicating that the preservation of edge features is better. The performance of SIIAWF[1] is shown in the last column of Table 4.1. It is observed that PSNR is increased on an average by 2.27dB compared to Qin et al (2010) and by 0.39dB compared to EAWF for US image1.

MSE had been phenomenally reduced for both the images. It has been reduced on an average of 40.6% than Qin et al (2010) and 8.32% than EAWF for US image1. The improvement in ENL measure is better at high (σ^2=0.1) variance. Another important parameter that shows a significant improvement is the EPI. It is increased on an average by 34.6% compared

with Qin et al (2010) and 2.64% compared to EAWF for US image 1. From these results it is evident that SIIAWF[1] performs better than the existing approaches in terms of noise reduction and in edge preservation. The qualitative performance of SIIAWF[1] is shown in Figure 4.6 for various noise variances. The noise reduction is good as seen by the visual inspection of the images.

The performance of SIIAWF[1] for US image 2 is analysed graphically as shown in Figure 4.7.The graphical analysis of US Image2 indicates that the present approach performs better than the other filters. Standard speckle filters produce again good noise reduction with less feature preservation. Also, the performance of Kuan and Lee filters overlapped mostly in all measures. For soft thresholding the performance is improved in terms of edge preservation than standard speckle filters. PSNR, MSE, ENL and SSIM values are improved for SIIAWF[1] compared to those of Qin et al (2010) approach and EAWF. EPI value is slightly reduced than Qin et al (2010) for low (0.01) and moderate (0.04) noise variances but increased for high variances (0.08 and 0.1).Hence the performance of SIIAWF[1] is observed to be better for US image2 also. Figure 4.8 presents the performance comparison of PSNR values for various window sizes. The result is good for smaller window size when noise level is increased. .

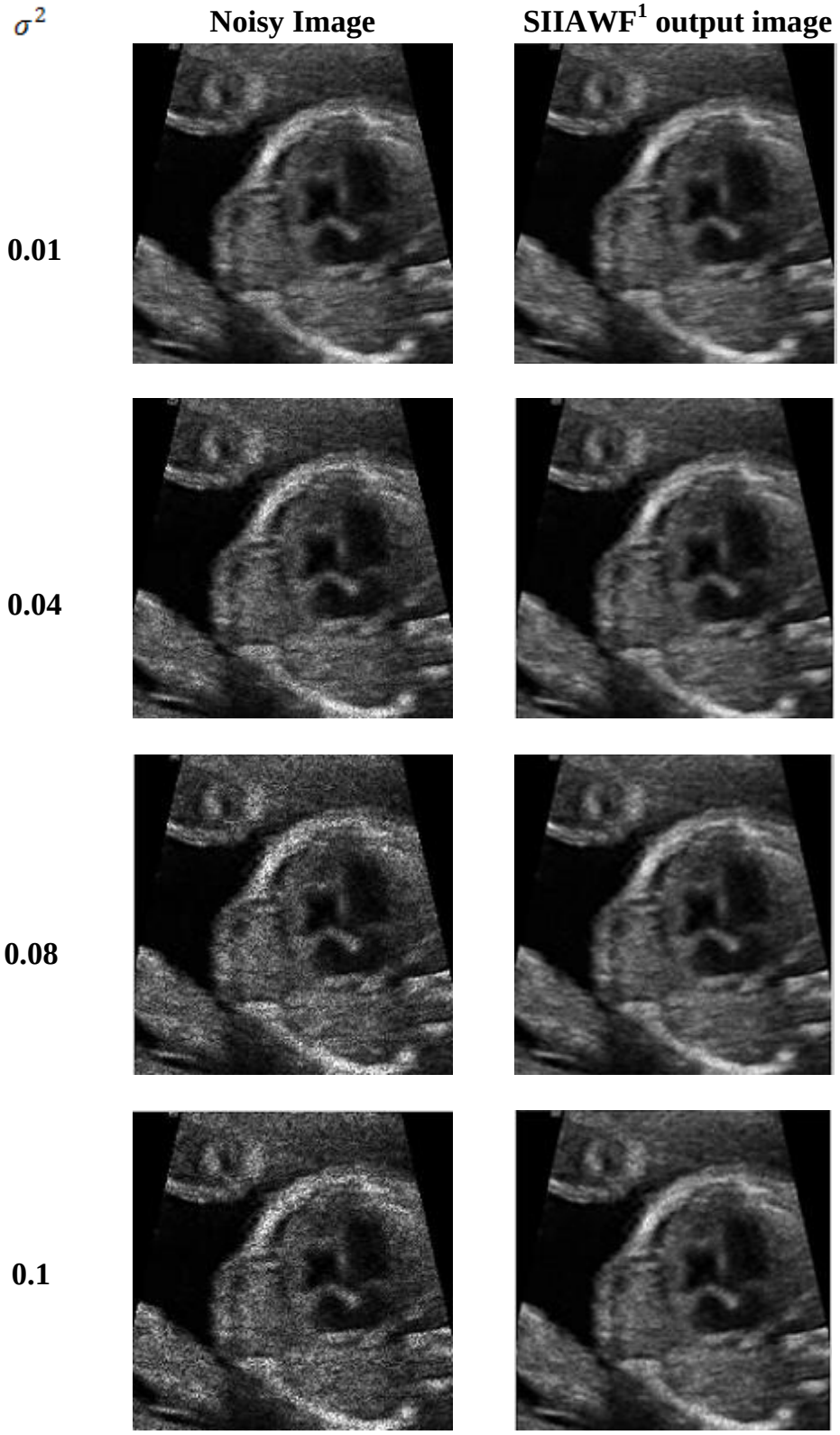

Figure 4.6 Comparison of visual quality of SIIAWF[1] for different noise variances for US image 1

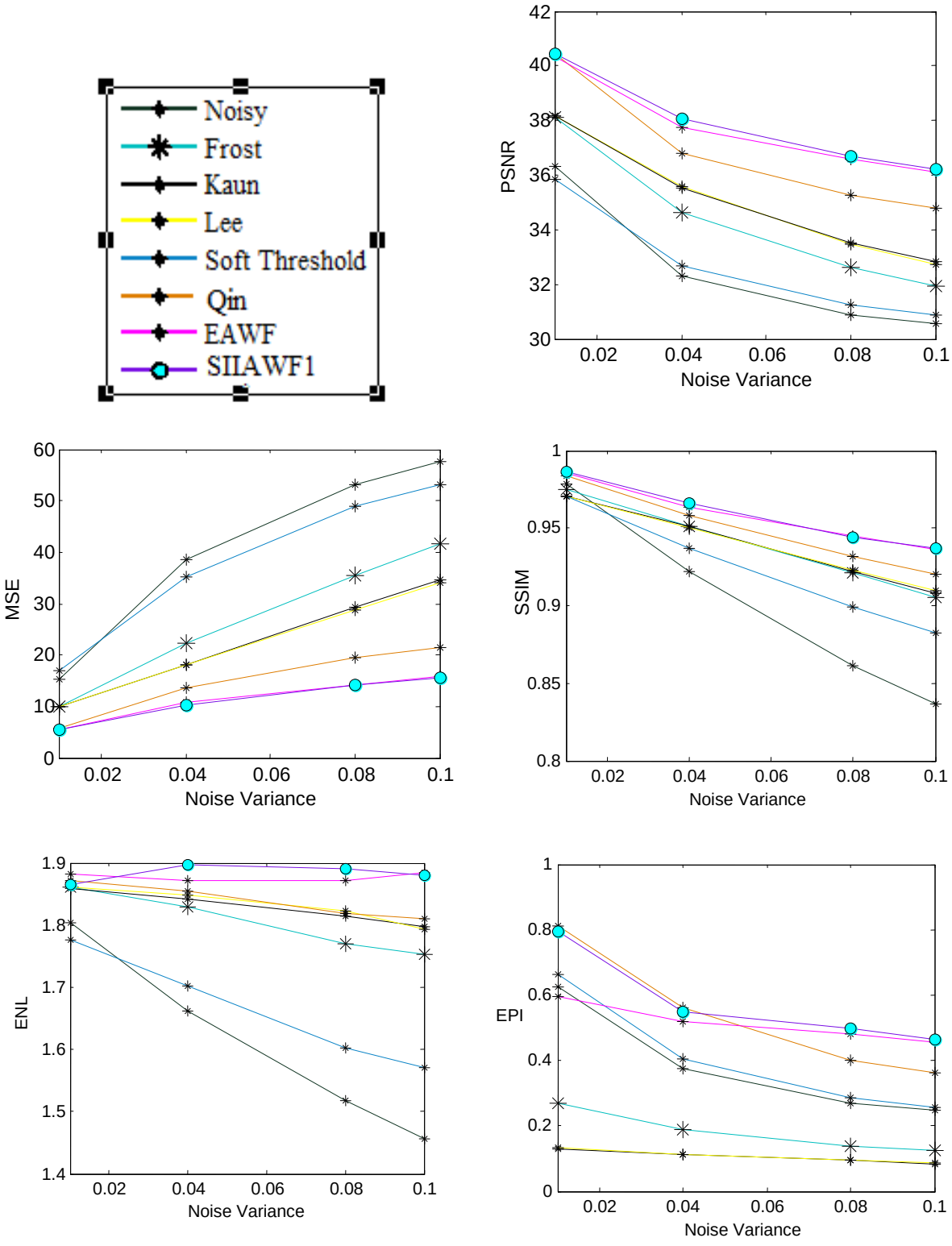

Figure 4.7 Graphical analysis of various performance measures of SIIAWF[1] for US image2

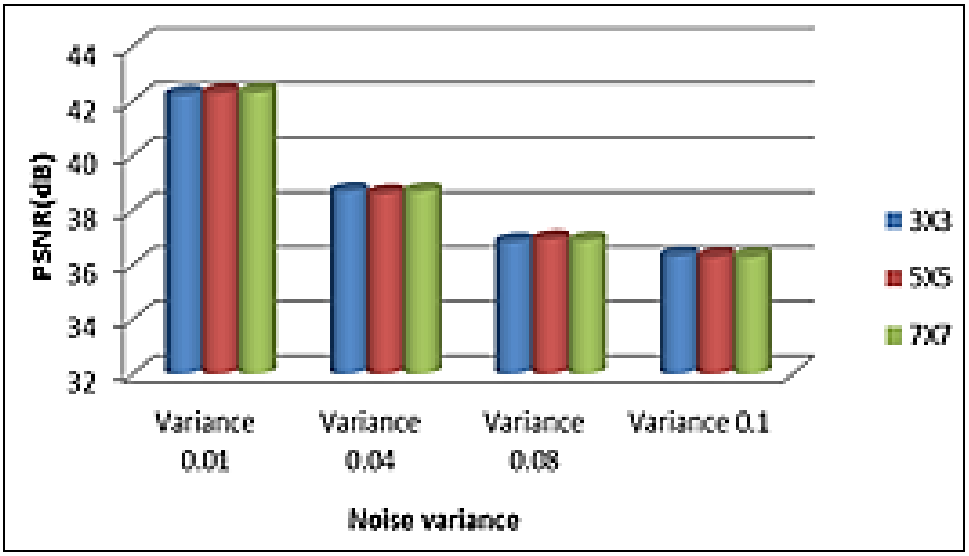

Figure 4.8 PSNR comparison of SIIAWF[1] for various window sizes and noise variances

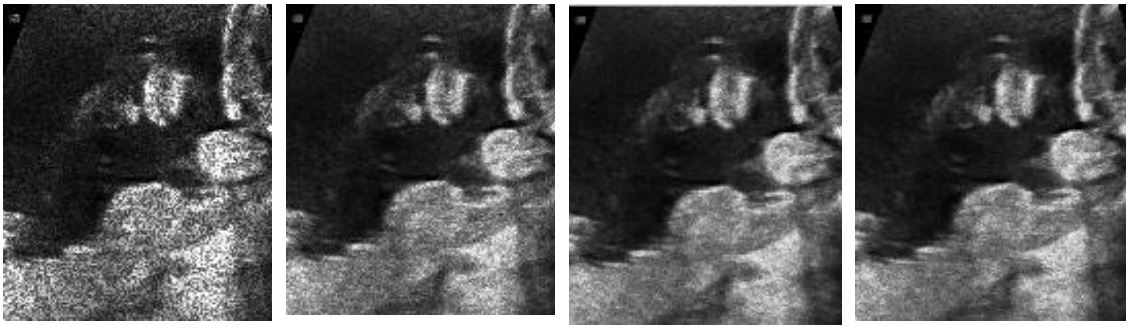

a. Noisy Image **b. Frost Filter** **c. Lee Filter** **d.Kuan Filter**

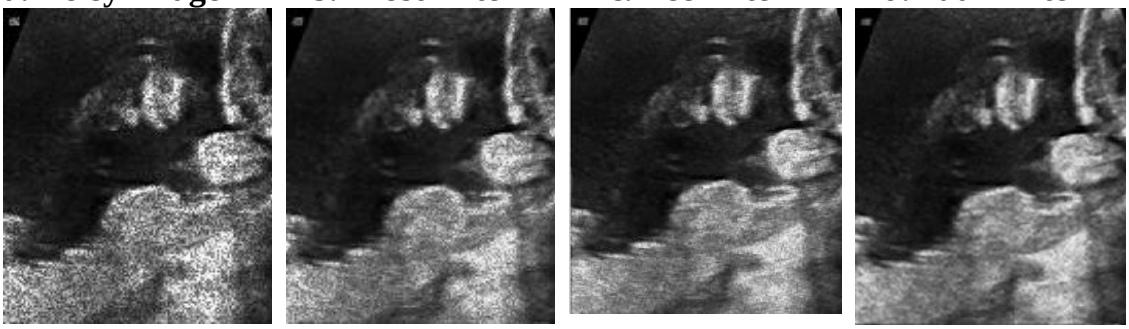

e. Soft Thresholding **f. Qin et al** **g. EAWF** **h. SIIAWF[1]**

Figure 4.9 Comparison of visual quality of SIIAWF[1] for US image3

Figure 4.9 shows the comparison of output image of SIIAWF[1] with outputs of existing filters for noise variance $\sigma^2 = 0.1$ when simulated with US image3. It is seen from Figure 4.9 (h) that noise is better removed and contrast is improved for SIIAWF[1] compared with other approaches. Therefore, it may be observed that the filter produces an improved performance for clinical US images both qualitatively and qualitatively.

In SIIAWF[1] the denoised coefficients better approximate the original coefficients, due to the reduction of fixed bias with the help of the proposed new and improved adaptive thresholding function. This is achieved by modifying the low magnitude coefficients between the thresholds $\lambda_{MB}/3$ and λ_{MB} as shown in the second line of the Equation (4.6). The adaptive threshold in SIIAWF[1] is determined using the intra-scale measure. As seen from Figure 4.3 the modelling of the coefficients with intra- scale measure based variance fits better than the ML and homogeneity based variances. Thus this intra scale measure serves as a good spatial adaptivity indicator aiding the filter to have a better feature preservation.

The approach defined for preliminary classification of signal of interest and noise coefficients exploiting multiscale product of the wavelet coefficients narrowed down the coefficients to be processed for estimating the parameters for threshold. This reduces the computational complexity yielding a better adaptive threshold. The truncation threshold defined for the determination of context facilitated the algorithm in retaining the original image features in the reconstructed image and hence improved edge preservation is achieved. The estimation of weighted signal variance resulted in a better threshold estimation, thus improving the noise removal performance. The results and comparisons indicate that the SIIAWF[1] performs better than the existing filtering approaches in noise removal as well as in preserving edges and fine details.

4.2 SHIFT INVARIANT IMPROVED ADAPTIVE WAVELET FILTER^2 (SIIAWF^2)

SIIAWF^2 performs a two stage thresholding. In the first stage a combined intra and inter-scale measure based signal variance estimation is proposed for adaptive threshold determination. In the second stage, the coefficients are further subjected to thresholding using a new error measure estimate and an adaptive thresholding function.

4.2.1 Block Diagram of SIIAWF^2

Figure 4.10 depicts the block diagram of the proposed filtering scheme SIIAWF^2

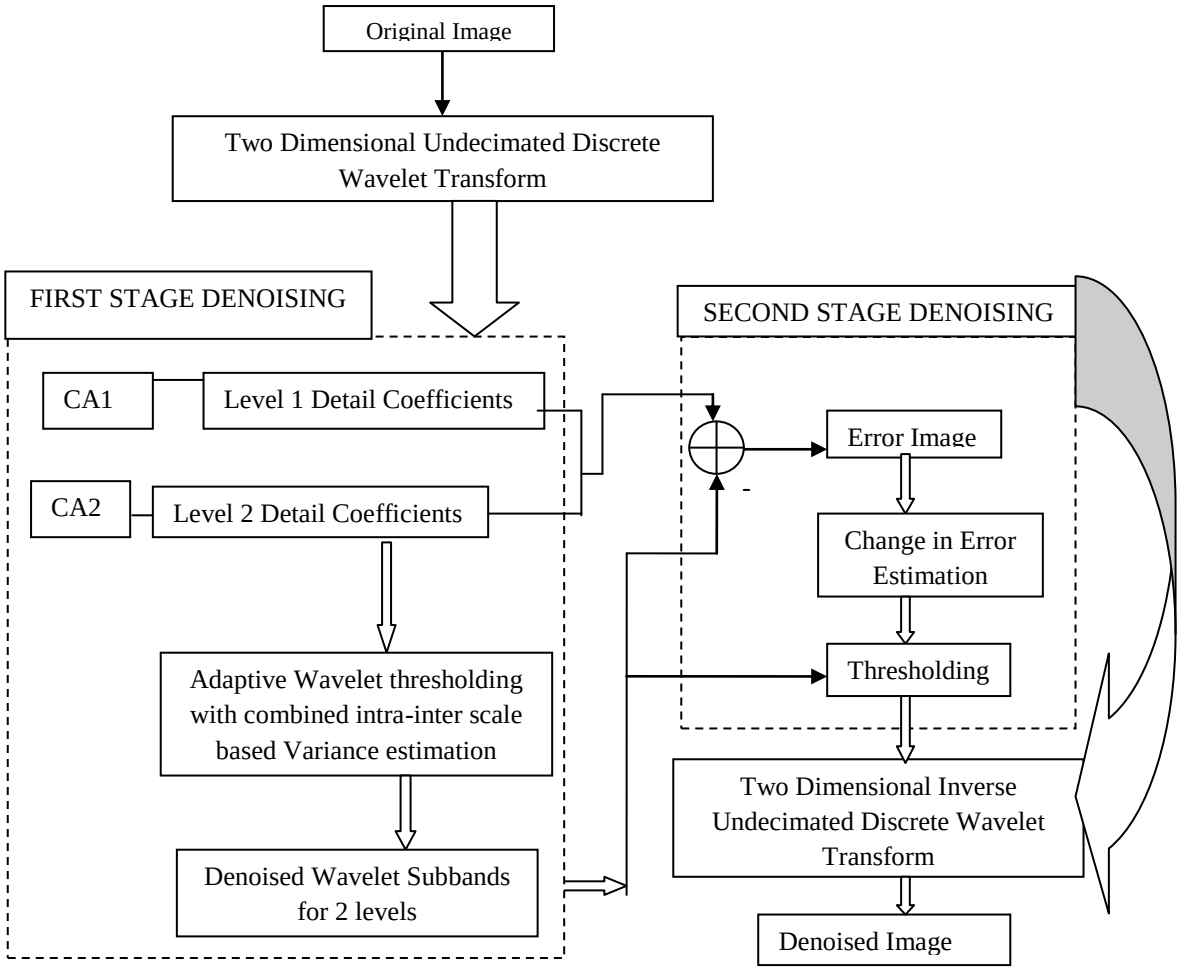

Figure 4.10 Block diagram of SIIAWF^2

4.2.2 First Stage Denoising of SIIAWF^2

A two dimensional undecimated discrete wavelet transform is applied to the input image to decompose the image into approximation and detail coefficients. Let $W^l(i,j)$ be the wavelet coefficients, where l represents the resolution scale. In Figure 4.10, CA1 and CA2 are the approximation coefficients of level 1 and level 2 decompositions respectively. The detail coefficients are then subjected to two stage thresholding. In the first stage, the detail coefficients are thresholded using the improved adaptive wavelet thresholding function defined in Equation (4.6) with a modified signal variance estimate. The following steps are carried out in the first stage denoising.

(i) Performing PCC

(ii) Determination of signal variance by a combined intra and inter-scale LSAM based estimate

(iii) Shrinking the wavelet coefficients

The procedure for PCC was explained in section 4.1.1. The proposed method for signal variance estimation is detailed below.

4.2.2.1 Proposed inter and intra-scale based signal variance estimation

The dependency of the wavelet coefficients in the adjacent subbands called inter scale dependency is used for signal variance estimation by many researchers in different ways. Pizurica (2002) used the inter-scale ratios to estimate roughly the local regularity of an image to make a distinction between useful edges and noise. In Malfait & Roose (1997) the ratio of the magnitudes of wavelet coefficients was averaged over a certain number of resolution scales. In SIIAWF^2, ML method of signal variance is modified exploiting inter

and intra-scale based LSAM. For the modified signal variance estimation σ_y^2 is estimated as,

$$\sigma_y^2 = \frac{1}{MN}\sum_{i=1}^{M}\sum_{j=1}^{N}\left(\frac{W^l(i,j)^2 + W^{l+1}(i,j)^2}{2*2^l}\right)\bullet E_T(i,j) \tag{4.7}$$

where MN is the size of the image and $W^l(i,j)$ and $W^{l+1}(i,j)$ are the subband coefficients at level l and $l+1$respectively, and E_T is the weight kernel defined in Equation (4.4). The signal variance is then estimated as in Equation (3.6). Figure 4.11 shows the pdfs of the histogram of the HH^1 subband. Figure 4.12 shows the pdf generated for HH_1 subband using the variances estimated through ML, homogeneity, intra-scale and the combined inter and intra-scale measures.

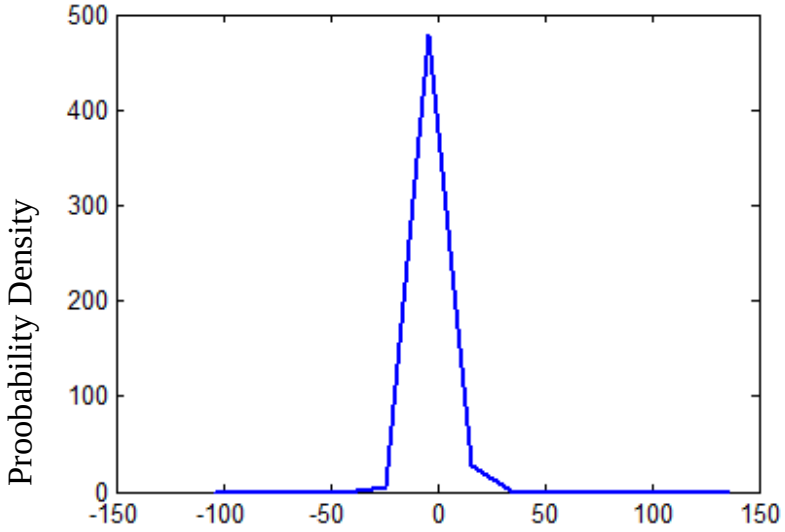

Figure 4.11 Histogram pdf of HH^1 subband

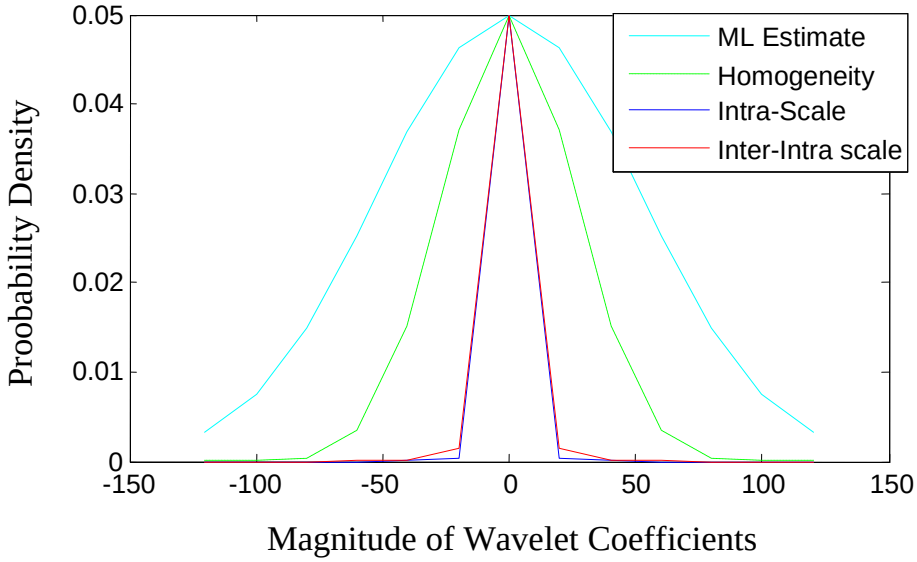

Figure 4.12 Comparison of pdfs' generated with ML, homogeneity, intra-scale and combined inter and intra-scale measure based variances

From Figures 4.11 and 4.12 it is observed that the pdf estimated through the proposed inter- scale measure based variance estimate best fits the histogram pdf compared with all the other estimates. This is because the local information regarding the spatial activity of the pixels is captured better by the proposed variance via the LSAM. It therefore offers better adaptive thresholds for each of the subbands. The proposed signal variance estimate thus gives an indication of the local variability of the pixels and helps in retaining the important image features with improved noise removal performance.

In the next step, the adaptive threshold (λ_{MB}) is determined as in section 3.2.3 using the new estimated signal variance. The wavelet coefficients are then subjected to thresholding using the improved adaptive threshold function defined in Equation (4.6). The process is repeated for all the detail subbands and the coefficients are shrunk. The output of the first stage is given to a second stage thresholding for further improving the filter performance.

4.2.3 Second Stage Thresholding of SIIAWF^2

The performance of SIIAWF is further improved by adapting the threshold function with the help of an error measure computed between the original subband coefficients and the denoised coefficients from the first stage. New types of thresholding functions have been developed in the literature with several shape tuning parameters for adaptation, Zhang (2001) and Nasri & Nezamabadi-pour (2009). The proposed second stage of SIIAWF^2 discusses a low complexity approach for adapting the thresholding function for minimizing the error. The threshold function is adapted by means of a simple change in error measure estimate, instead of complex computations involved in neural network.

4.2.3.1 Calculation of change in error

Figure 4.13 shows the procedure for calculating the change in error measure. The adaptation in the threshold function is obtained by modifying the thresholding function depending on the sign of change in error measure. The error image $E(i, j)$ is obtained by subtracting the original sub-band coefficients and the first stage denoised coefficients.

$$E(i, j) = W'(i, j) - W(i, j) \tag{4.8}$$

where $W'(i, j)_1$ is the thresholded detail subband coefficients from first stage and $W(i, j)$ is the original detail subband coefficients. To determine the change in error measure the maximum of the error magnitude (E_m) is to be found out.

$$E_m = \max(|E(i, j)|) \tag{4.9}$$

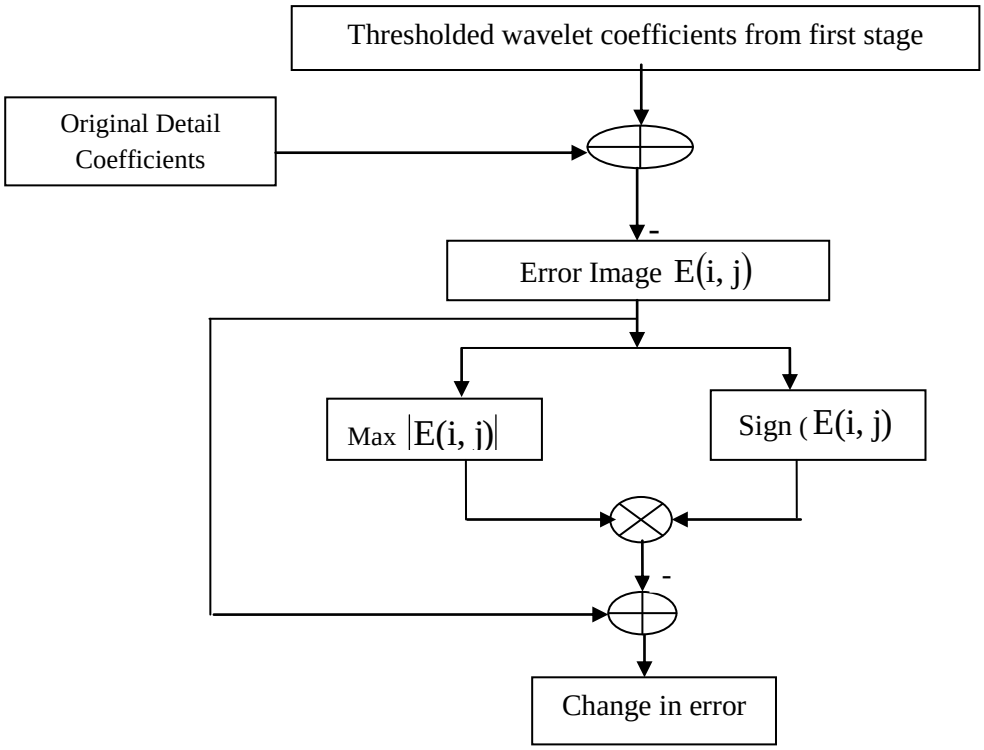

Figure 4.13 Calculation of change in error

The sign of each pixel location of the error subbands is determined.

$$sgn(i, j) = sign(E(i, j)) \tag{4.10}$$

The product of the maximum error magnitude and the sign of each pixel in the error subbands are used as a reference ($esgn(i, j)$) for determining the change in error.

$$esgn(i, j) = E_m * sgn(i, j) \tag{4.11}$$

The change in error for each subband coefficient is then determined as

$$\text{change in error}\,(\Delta e) = esgn(i, j) - E(i, j) \tag{4.12}$$

Thus, the change in error is obtained for all the detail coefficients.

4.2.3.2 New adaptive wavelet thresholding function

As discussed in the previous section the thresholding functions are adapted using several tuning parameters to reduce the error. This section describes a simple and an efficient adaptive thresholding function involving a change in error measure estimate. Based on the change in error measure determined in section 4.2.3.1, the coefficients are subjected to thresholding as defined in Equation (4.13)

$$\hat{W}(i,j) = \begin{cases} W'(i,j) + \dfrac{1}{MxN}\sum_{i=1}^{M}\sum_{j=1}^{N}\left(W(i,j)-\mu\right) & \text{if} \quad \text{sign}(\Delta e) \text{ is positive} \\ W'(i,j) & \text{if} \quad \text{sign}(\Delta e) \text{ is zero} \\ W'(i,j) - \dfrac{1}{MxN}\sum_{i=1}^{M}\sum_{j=1}^{N}\left(W(i,j)-\mu\right) & \text{if} \quad \text{sign}(\Delta e) \text{ is negative} \end{cases} \tag{4.13}$$

where $\hat{W}(i,j)$ is the final denoised coefficients and μ is the mean of the subband coefficients.

The process is repeated for all the subband coefficients. Inverse wavelet transform is then applied to obtain the reconstructed image.

4.2.4 Summary of the Denoising Algorithm for SIIAWF[2]

The proposed wavelet denoising algorithm is summarized as follows:

Step 1: The UDWT is applied on the input image to the required L resolution levels

Step 2: For each scale of decomposition 2^l, l= 1…L-1

For each detail orientation (HL, LH and HH),

- The mask, $\hat{I}(i,j)$ using inter-scale dependency is determined using Equation (4.1)
- Each detail subband is multiplied with its corresponding mask
- Noise variance is determined using Equation (3.2)
- Compute the signal variance using Equation (3.6) by
  - * Computing the edge threshold using Equation (4.3)
  - * Calculating the weight kernel using Equation (4.4)
  - * Calculation of σ_y^2 using Equation (4.7)
- Calculate the threshold T_{MB} using Equation (3.13) to Equation (3.15)
- Apply thresholding using the shift invariant improved adaptive thresholding function as in Equation (4.6) for each detail subband

Step 3 : For each scale of decomposition 2^l, l= 1…L-1

- For each orientation (HL,LH,HH),
  - Find the Error Image $E(i,j)$ using Equation (4.8)
  - Find the magnitude of maximum value of $E(i,j)$ using Equation (4.9)
  - Determine the sign of $E(i,j)$ using Equation (4.10)
  - Find the reference measure using Equation (4.11)
  - Determine the change in error using Equation (4.12)
  - Apply thresholding using Equation (4.13)

Step 4: Take inverse undecimated discrete wavelet transform

4.2.5 Results and Discussion

The simulation environment is the same as in EAWF and SIIAWF[1]. SIIAWF[2] is tested with synthetic phantom image and clinical US images shown in Figure 3.6 to Figure 3.8 for different noise variances.The performance of SIIAWF[2] is compared with standard despeckling filters (Lee, Frost and Kuan), soft thresholding, EAWF and SIIAWF[1]. The quantitative performance is evaluated with various measures like PSNR, MSE, SSIM, ENL and EPI. The qualitative performance is compared through visual quality evaluation.

The simulation outputs for noisy phantom images are shown below in Figure 4.14. From Figure 4.14, it is seen that the visual quality of SIIAWF[2] is better than the other filters considered. It is noted that the noise removal ability of the filter is improved compared to the standard speckle filters. In, SIIAWF[2] the noise removal ability, edge preservation and contrast are improved better compared with Soft thresholding approach. From Figure 4.14 (g) it is visualized that the image is smoothened in Qin et al (2010). The visual quality of SIIAWF[2] is better than EAWF and SIIAWF[1] interms of noise removal characteristics. The edges are also preserved better than Qin et al (2010). The visual quality of SIIAWF[2] is comparatively improved than EAWF and SIIAWF[1].

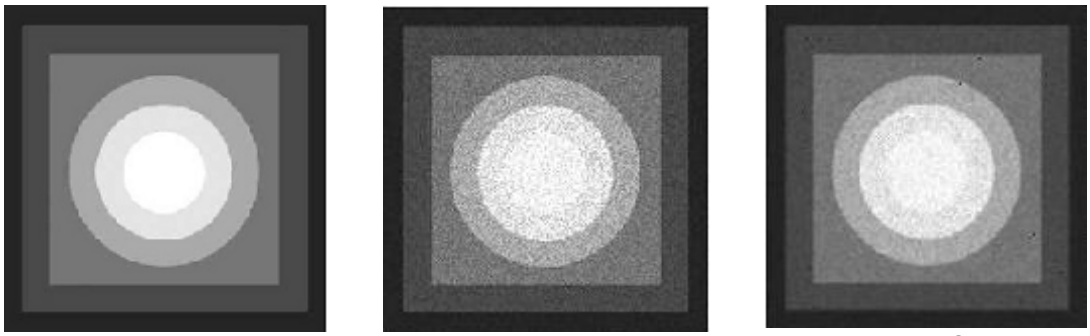

a. Original image

b. Noisy image

c. Frost filter

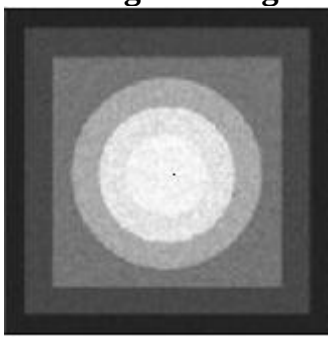

d. Kuan filter

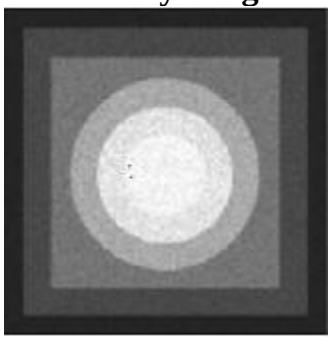

e. Lee filter

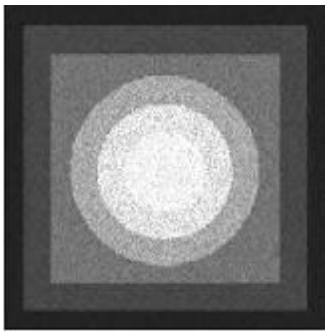

f.Soft Thresholding

g. Qin et al

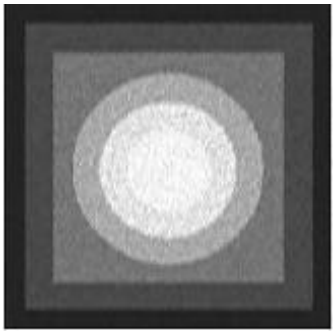

h. EAWF

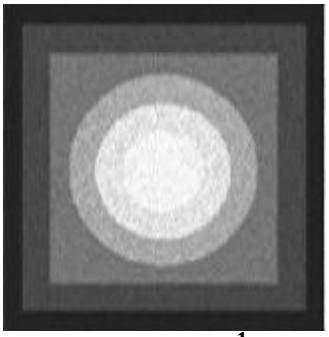

i. SIIAWF[1]

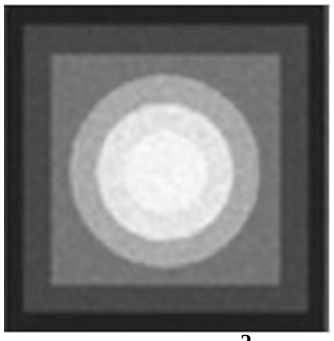

j. SIIAWF[2]

Figure 4.14 Comparison of visual quality of SIIAWF[2] with various filters for synthetic phantom image

Table 4.3 Performance comparison of SIIAWF^2 for different noise variances and filters

σ^2	Noisy	Frost	Kuan	Lee	Soft	Qin	EAWF	SIIAWF^1	SIIAWF^2
	Peak Signal to Noise Ratio								
0.01	34.9435	38.6438	39.8387	39.7923	36.2507	40.4068	41.8515	42.2175	**44.4192**
0.04	31.4191	34.0636	35.5479	35.5193	33.1247	36.0805	38.4214	38.5345	**40.0198**
0.08	30.4078	31.8946	32.9930	32.8841	32.0909	34.4780	36.4853	36.8641	**38.3227**
0.1	30.1131	31.2677	32.0888	32.0758	31.7935	34.0053	35.7670	36.4357	**37.8468**
	Mean Square error								
0.01	20.8321	8.8859	6.7485	6.8211	15.4175	5.9210	4.2455	3.9024	**3.0004**
0.04	46.8998	25.5104	18.1254	18.2455	31.6673	16.0335	9.3528	9.1124	**7.5154**
0.08	59.1965	42.0362	32.6425	33.4712	40.1782	23.1889	14.6068	13.3866	**10.2651**
0.1	63.3536	48.5639	40.1979	40.3180	43.0259	25.8553	17.2337	14.7745	**11.1274**
	Structural Similarity Index Measure								
0.01	0.9663	0.9804	0.9819	0.9820	0.9666	0.9822	0.9848	0.9854	**0.9889**
0.04	0.8882	0.9451	0.9512	0.9515	0.9135	0.9461	0.9608	0.9612	**0.9655**
0.08	0.8104	0.9023	0.9145	0.9124	0.8559	0.9068	0.9346	0.9377	**0.9499**
0.1	0.7815	0.8798	0.8944	0.8938	0.8311	0.8913	0.9210	0.9285	**0.9419**
	Equivalent Number of Looks								
0.01	1.6661	1.7021	1.6975	1.6994	1.6419	1.7094	1.7114	1.7131	**1.7430**
0.04	1.5483	1.6716	1.6844	1.6848	1.5643	1.6865	1.7125	1.7204	**1.7565**
0.08	1.4127	1.6304	1.6648	1.6636	1.4767	1.6631	1.7081	1.7286	**1.7515**
0.1	1.3606	1.6065	1.6564	1.6593	1.4347	1.6495	1.7013	1.7247	**1.7466**
	Edge Preservation Index								
0.01	0.3274	0.2622	0.2244	0.2213	0.3486	0.5470	0.5766	0.5979	**0.6752**
0.04	0.1722	0.1552	0.1646	0.1628	0.1759	0.2837	0.4285	0.4417	**0.5410**
0.08	0.1239	0.1085	0.1312	0.1262	0.1221	0.1966	0.3598	0.3407	**0.5051**
0.1	0.1114	0.0974	0.1100	0.1121	0.1072	0.1763	0.3308	0.3387	**0.4922**

Table 4.3 shows the comparison of various quantitative measures for different noise variances and filters for US image 1.The results of simulation carried out with different wavelet functions for noise variance 0.01 are shown in Table 4.4.

Table 4.4 Comparison of performance metrics of SIIAWF^2 for different wavelets

Wavelets / Metrics	dB4	Coif3	Sym2	haar	Bior 1.1
PSNR(dB4)	44.4192	43.9240	**44.4958**	42.3863	42.4409
MSE	3.0004	2.6344	**2.2935**	3.7536	3.7067
SSIM	**0.9889**	0.9882	**0.9889**	0.9801	0.9874
EPI	**0.6752**	0.6215	0.6646	0.4724	0.4760
ENL	1.7430	1.7465	1.7432	1.7516	1.7477

The value of PSNR is high for Sym2 by 0.08dB compared to db4. But for db4 the value of SSIM and EPI are better than Sym2. This indicates that the preservation of image feature is better with db4. Hence db4 wavelet is used for simulation of results in Table 4.3. From Table 4.3, it is observed that the proposed SIIAWF^2 performs better than the existing spatial and wavelet domain filters considered for comparison. It is seen from Table 4.3 that PSNR is increased on an average by 6.84dB compared to soft thresholding, 3.91dB compared to Qin et al (2010) approach, 2.02dB compared to EAWF and 1.64dB compared to SIIAWF^1 for US image1. MSE has been reduced on an average up to 53.79% than Qin et al (2010) approach, 28.53% than EAWF and 22.16% than SIIAWF^1 for US image1. The parameter EPI is increased on an average by 47.95% compared with Qin et al (2010), 24.24% than EAWF and 23.38% than SIIAWF^1 for US image 1. The value of SSIM is also increased along with ENL measure improvement.

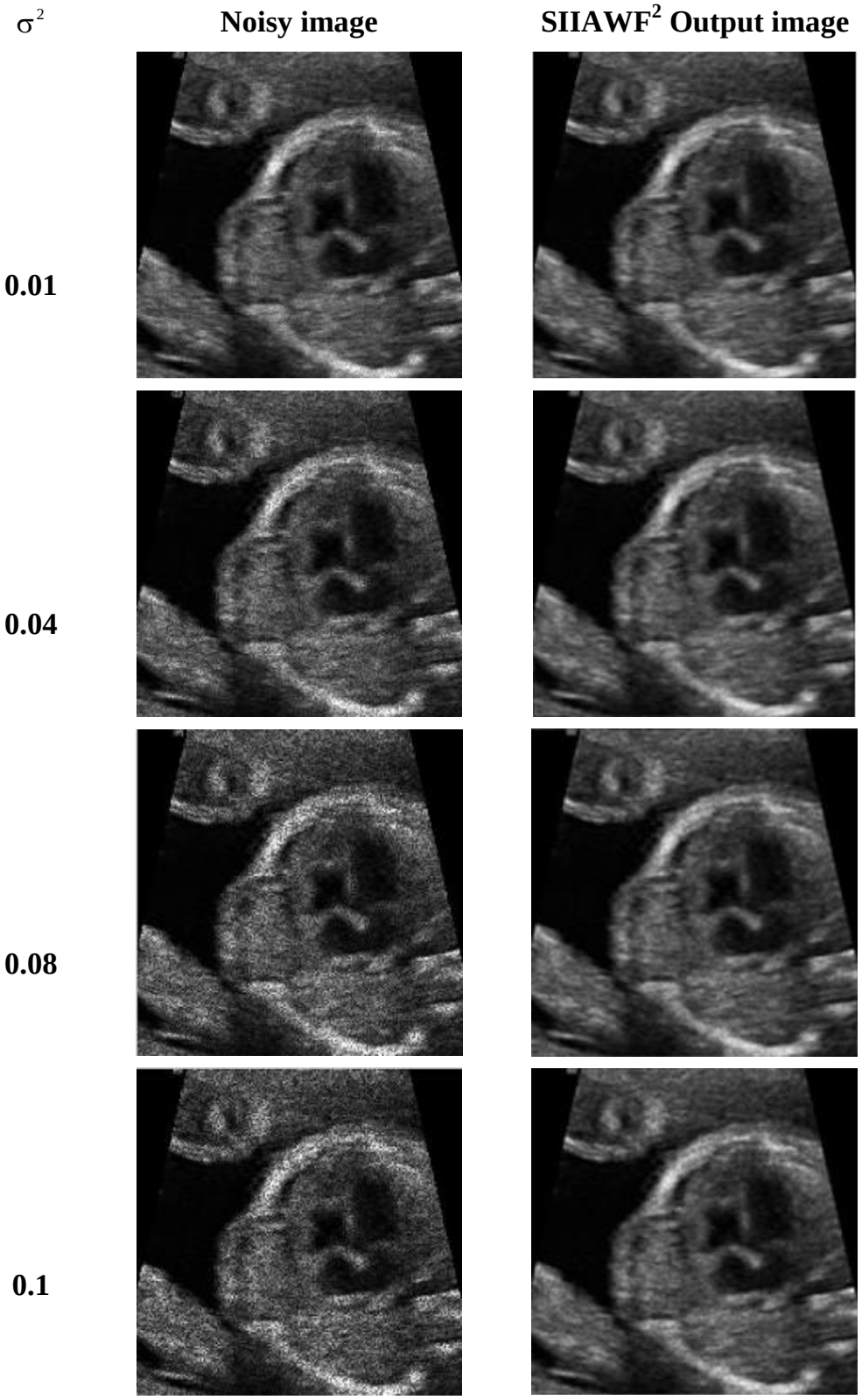

Figure 4.15 Comparison of visual quality of SIIAWF^2 for different noise variances for US image1

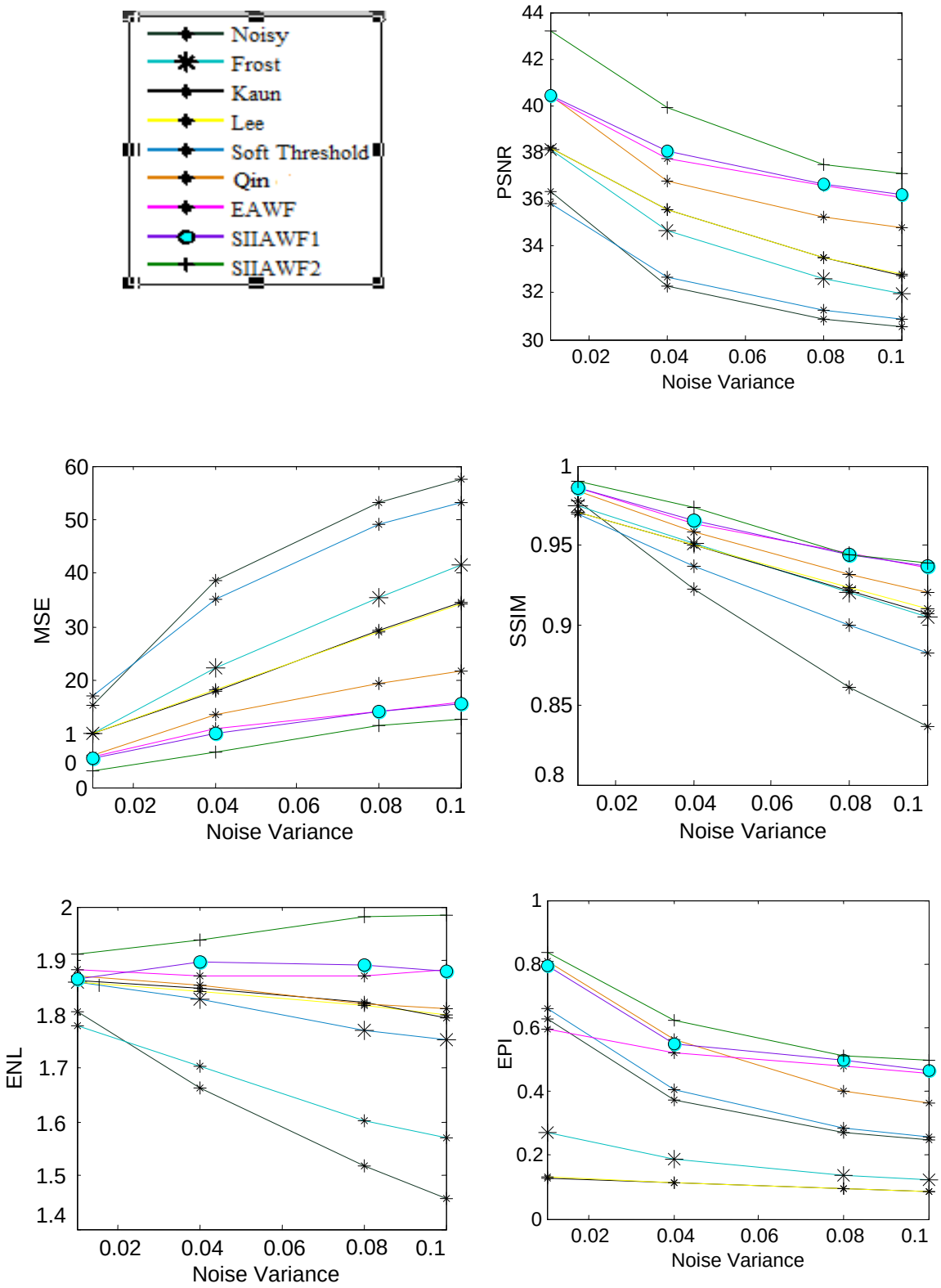

Figure 4.16 Graphical analysis of various performance measures of SIIAWF^2 for US image2

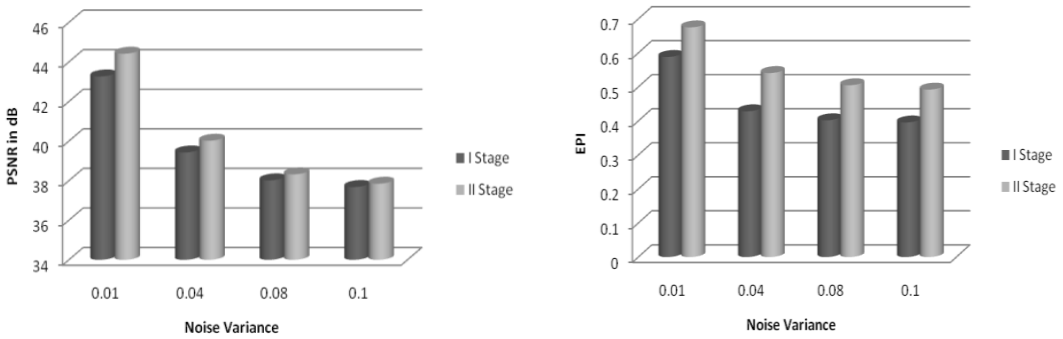

Figure 4.17 Comparison of PSNR and EPI between the two stages of SIIAWF[2]

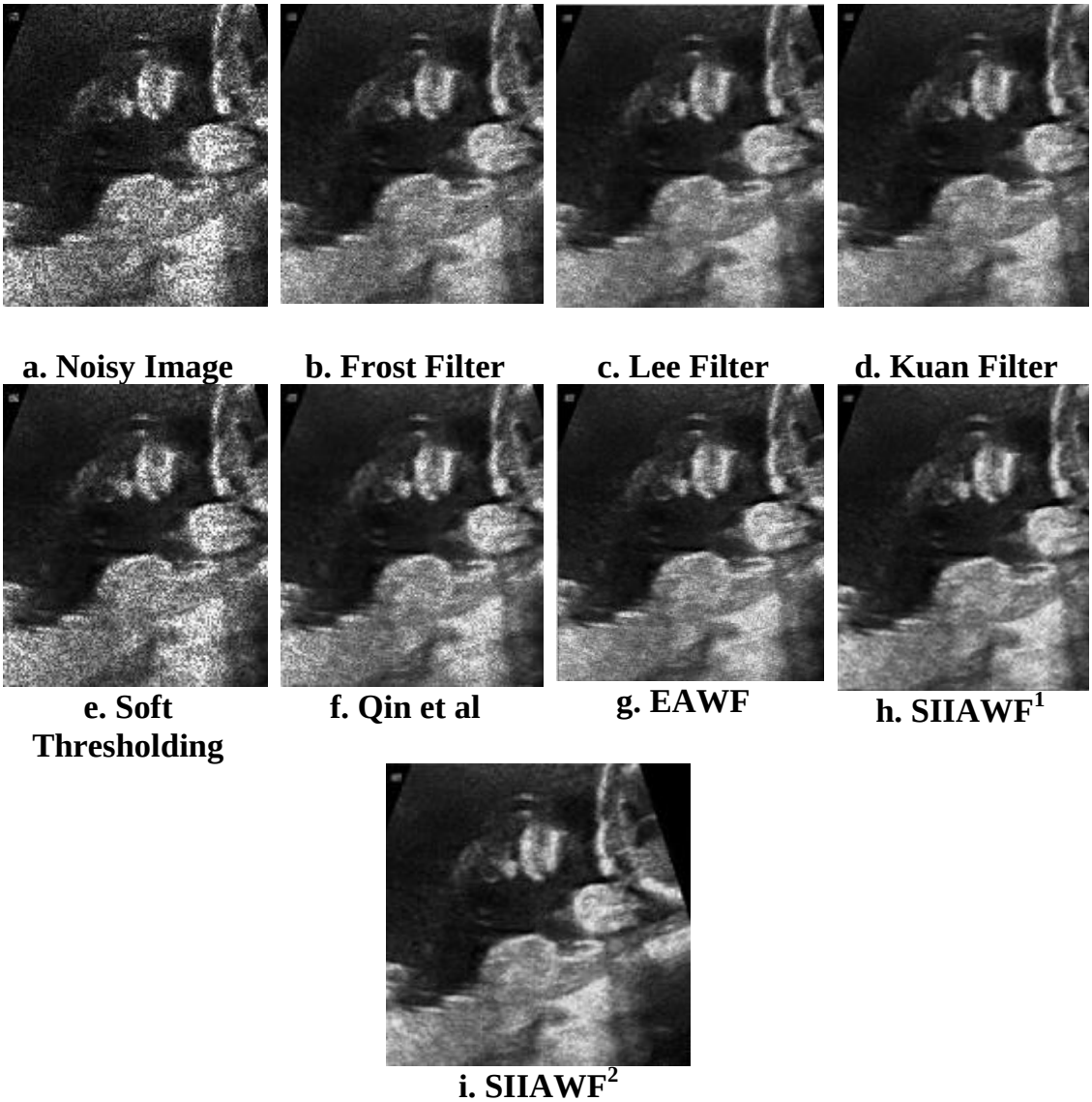

a. Noisy Image **b. Frost Filter** **c. Lee Filter** **d. Kuan Filter**

e. Soft Thresholding **f. Qin et al** **g. EAWF** **h. SIIAWF[1]**

i. SIIAWF[2]

Figure 4.18 Comparison of visual quality of SIIAWF[2] with existing filters for US image3

Hence from Table 4.3 it is seen that a significant improvement in noise reduction is achieved by SIIAWF^2 compared to the spatial domain filters along with improved feature preservation. Compared to the approaches EAWF and SIIAWF^1 the PSNR is increased significantly for low as well as high noise variances, whereas EPI measure shows a significant improvement for high noise variance in SIIAWF^2. Figure 4.15 illustrates the comparison of visual quality of the output images of SIIAWF^2 for different noise variances and it is visualized that the output image quality is improved for varying noise conditions.

Figure 4.16 shows the graphical analysis of performance of SIIAWF^2 for clinical US image2 and it is seen that SIIAWF^2 outperforms other filters in all aspects. PSNR value is boosted better compared to EAWF and SIIAWF^1. The value of SSIM for SIIAWF^2 is closer to SIIAWF^1 for high noise variance. The performances of Lee and Kuan filters overlap for all metrics. Figure 4.17 presents the performance comparison of PSNR and EPI metrics between the two stages of the proposed SIIAWF^2 for various noise variances. It is seen that the preservation of image features is improved in the second stage. Visual quality improvement of the Clinical US image3 is shown in Figure 4.18, for the various approaches. Figures 4.18(b)–(f) show the output of the standard speckle filters, soft thresholding and Qin et al (2010) approach. It is seen from the output images that noise is not completely removed. Comparing the output images in Figures 4.18(g) – (i), it is clear that visual quality of SIIAWF ^{2} in Figure 4.18 (i) is enhanced better than all the other filters considered.

4.3 SUMMARY

In this chapter two frameworks of Shift Invariance Improved Adaptive Wavelet Filter (SIIAWF) have been discussed. The first framework SIIAWF^1 perform speckle reduction using a new and improved adaptive

thresholding function with intra-scale measure based signal variance estimation. The second framework SIIAWF^2 performs a two stage filtering. First, a combined inter and intra-scale measure based signal variance is estimated and thresholding is done with the new and improved adaptive thresholding function. Then, the denoised coefficients are further subjected to thresholding with a new adaptive thresholding function, based on a change in error measure.

The property of wavelets, edge evolution across scales is utilized to form preliminary coefficient classification and it helps in retaining the edges and fine details. The new and improved adaptive wavelet thresholding function reduced the fixed bias between the original and reconstructed coefficients and also reduced the number of zero coefficients. Hence the reconstructed coefficients approximated the original coefficients. The weight kernel determined from the sample mean absolute deviation of the data from their mean gave a good indication of the local variability of the coefficients. Hence, the intra- scale variance estimate provided a better adaptation to the threshold and resulted in an improved performance of SIIAWF^1. In SIIAWF^2 the combined intra and inter-scale variance estimate incorporated the local information using the inter scale dependencies also. This gave an improved spatial adaptivity indication of the pixels and resulted in better adaptive threshold. Edge clustering property of wavelet, is exploited to form the LSAI, within a subband. Hence the important image edges are retained better. The performance of the filter is further improved by adapting the thresholding function with respect to the error measure. The change in error measure calculated thus reduced the noise further and retained the original information better.